

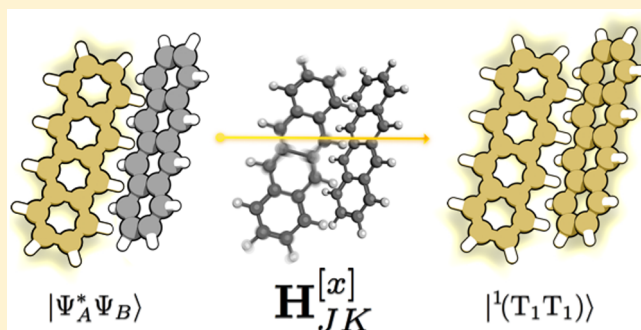
Evidence for Singlet Fission Driven by Vibronic Coherence in Crystalline Tetracene

Adrian F. Morrison and John M. Herbert*[✉]

Department of Chemistry and Biochemistry, The Ohio State University, Columbus, Ohio 43210, United States

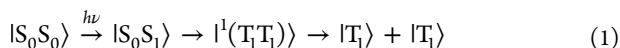
S Supporting Information

ABSTRACT: Singlet fission proceeds rapidly and with high quantum efficiency in both crystalline tetracene and pentacene, which poses a conundrum given that the process in tetracene is disfavored by the electronic energetics. Here, we use an *ab initio* exciton model to compute nonadiabatic couplings in the unit cell of tetracene in order to identify the modes that promote this process. Four intramolecular modes in the range of 1400–1600 cm^{-1} , which are nearly resonant with the single-exciton/multiexciton energy gap, appear to play a key role. *Ab initio* calculations of the electron/phonon coupling constants for these modes reveal that they are almost entirely of “Holstein” type, modulating the site energies rather than the intersite couplings. The constants are used to parametrize a vibronic Hamiltonian, simulations with which suggest a vibronically coherent singlet fission mechanism that proceeds spontaneously despite unfavorable electronic energetics. In the absence of vibronic coupling, there is no significant fission according to our model.



Singlet fission^{1,2} (SF) offers the potential for enhanced solar energy conversion by overcoming the Shockley–Queisser efficiency limit of 30% for single-junction solar cells,³ by means of harvesting states excited by high-energy photons that would otherwise vibrationally cool before electron transfer could occur. The SF process has been observed in acene derivatives, carotenoids, and other conjugated systems, often on an ultrafast time scale and with unit quantum yield for generation of the “multiexciton” state, $|^1(T_1T_1)\rangle$. Pentacene-based devices with external quantum efficiencies (ratio of charge carriers to incident photons) of 129% have been reported.⁴

The generally accepted mechanism for SF is²



In crystals of pentacene and its derivatives, $2E(T_1) < E(S_1)$ so that SF is energetically favorable, and the process is observed to occur on a time scale of 80–100 fs.^{5,6} Theoretical studies, however, indicate that direct electronic coupling between $|S_0S_1\rangle$ and $|^1(T_1T_1)\rangle$ is too weak to be consistent with such a fast time scale.^{7,8} Moreover, SF occurs spontaneously in crystalline tetracene as well,^{9–11} with high quantum efficiency and (at certain excitation energies) on a subpicosecond time scale,^{9,10} despite the fact that $2E(T_1)$ lies approximately 0.2 eV above $E(S_1)$ in tetracene.^{7,12,13} Several mechanisms have been proposed to explain this, including thermally activated SF from a vibrationally hot S_1 state, fission from higher-lying S_n states,⁷ or an entropically driven mechanism.¹⁴ However, these hypotheses are difficult to reconcile with observations that the SF rate is independent of temperature in tetracene¹⁰ (or

perhaps nearly so, with an activation energy of ~ 0.06 eV¹⁵) and also insensitive to excitation energy.¹¹ Here, we propose a mechanism to explain SF in tetracene based on a Holstein–Peierls vibronic Hamiltonian,^{16,17} with parameters derived from *ab initio* calculations.

Recently, Zhu and co-workers reported direct observation of the $|^1(T_1T_1)\rangle$ state using time-resolved two-photon photoemission.¹⁸ These authors report a ~ 20 fs rise time in the triplet population in both tetracene and pentacene, which they attribute to formation of the multiexciton state. Although others have attributed this signal to free triplet excitons,¹⁹ Zhu et al. propose a quantum-coherent mechanism in which the initial photoexcited state is a superposition with singlet as well as multiexciton character.^{14,18} A phenomenological density matrix simulation reproduced the ultrafast rise time in the $|^1(T_1T_1)\rangle$ population when charge-transfer (CT) states were included to mediate the process.¹⁸ However, the phenomenological calculations in support of this mechanism^{14,18} have been criticized as requiring interactions with a bath, the demand for which cannot explain the temperature independence of the SF rate.²⁰ Finally, the precise role of CT states in SF has been debated,^{1,2,21} with some consensus emerging that these states lie too high in energy to be directly accessed but that the presence of CT character in the single- and multiexciton states serves as a virtual intermediate, where the CT character contributes to the coupling of the adiabatic states.^{8,18,21–24}

Received: January 29, 2017

Accepted: March 9, 2017

Published: March 9, 2017

The role of the nuclear degrees of freedom has only recently garnered attention, with two theoretical studies identifying a crossing point on the Born–Oppenheimer potential energy surfaces for the single- and multiexciton states in pentacene,^{7,22} leading to a proposed mechanism involving a conical intersection along an intermolecular “herringbone” coordinate. Indeed, Musser et al.⁶ report direct experimental evidence for SF through a conical intersection in pentacene, driven by high-frequency vibrational modes, but no such evidence has been reported for tetracene. The study in ref 7 failed to find any such intersection along the corresponding herringbone coordinate in tetracene.

A crucial quantity to describe nonadiabatic transitions through conical intersections is the derivative coupling vector

$$\mathbf{d}^{JK} = \langle \Psi_J | \hat{\nabla} | \Psi_K \rangle \quad (2)$$

where $\hat{\nabla}$ represents derivatives with respect to nuclear coordinates. This can be related to the nonadiabatic coupling vector

$$\mathbf{h}^{JK} = \langle \Psi_J | (\partial \hat{H} / \partial x) | \Psi_K \rangle = (E_J - E_K) \mathbf{d}^{JK} \quad (3)$$

These quantities describe the topography and topology around conical intersections and can be said to “drive” nonadiabatic processes.

Derivation and implementation of \mathbf{h}^{JK} vectors is technically involved for any electronic structure model, and the difficulty is compounded in the context of SF by the doubly excited character of the $|^1(T_1 T_1)\rangle$ state. Popular low-cost methods such as time-dependent density functional theory do not capture double excitations²⁵ and are therefore blind to the $|^1(T_1 T_1)\rangle$ intermediate. Using methods that do incorporate double excitations but using the norm of the single-particle transition density matrix as a proxy for \mathbf{h}^{JK} because the latter is unavailable, Krylov and co-workers have suggested that the nuclear modes that serve to increase electronic coupling do not always increase the nonadiabatic couplings.^{22,26,27}

We have recently introduced a novel approach for computing excited-state properties of extended aggregates, based on an *ab initio* Frenkel–Davydov exciton model (AIFDEM).^{28–30} The Frenkel–Davydov *ansatz* writes the wave function $|\Xi_I\rangle$ for a collective excitation as a linear combination of direct products of monomer states:

$$|\Xi_I\rangle = \sum_A^{\text{states}} K_{IA} |\Psi_A^* \Psi_B \Psi_C \dots\rangle \quad (4)$$

where $|\Psi_M\rangle$ and $|\Psi_M^*\rangle$ are ground- and excited-state wave functions for the M th monomer. This set of direct products is known as the “exciton-site basis”. Both of these states, and the coupling matrix elements between them, can be computed in a trivially parallelizable way. Unlike traditional Frenkel–Davydov models, the AIFDEM need not invoke dipole coupling, nearest-neighbor, neglect-of-exchange, frontier orbital, or other approximations to the electronic Hamiltonian that couples the basis states.²⁸

As in our previous work on the AIFDEM,^{28,29} we will describe the monomer wave functions using only single excitations, but for SF, we also need to include multiexciton configurations by coupling two triplet monomer wave functions to an overall singlet. (A somewhat similar approach was recently used to parametrize a lattice model for SF.³¹) Starting

from a direct product that includes two fragments in triplet configurations, the additional exciton-site basis states that we need are

$$\begin{aligned} |^1(\Psi_A^T \Psi_B^T) \Psi_C \dots\rangle &= \frac{1}{\sqrt{3}} |\Psi_A^{T_{+1}} \Psi_B^{T_{-1}} \Psi_C \dots\rangle \\ &+ \frac{1}{\sqrt{3}} |\Psi_A^{T_{-1}} \Psi_B^{T_{+1}} \Psi_C \dots\rangle - \frac{1}{\sqrt{3}} |\Psi_A^{T_0} \Psi_B^{T_0} \Psi_C \dots\rangle \end{aligned} \quad (5)$$

where $\Psi_M^{T_m}$ is a triplet wave function on monomer M , with magnetic quantum number m :

$$|\Psi_M^{T_{+1}}\rangle = \sum_{ia} t^{ia} |\Phi_M^{\bar{1}a}\rangle \quad (6a)$$

$$|\Psi_M^{T_{-1}}\rangle = \sum_{ia} t^{ia} |\Phi_M^{\bar{1}\bar{a}}\rangle \quad (6b)$$

$$|\Psi_M^{T_0}\rangle = \frac{1}{\sqrt{2}} \sum_{ia} t^{ia} (|\Phi_M^{ia}\rangle - |\Phi_M^{\bar{1}\bar{a}}\rangle) \quad (6c)$$

Hamiltonian and overlap matrix elements between exciton-site basis functions are computed as described in our previous work,^{28,29} and we then solve a generalized the eigenvalue problem

$$\mathbf{H}\mathbf{K}_I = \epsilon_I \mathbf{S}\mathbf{K}_I \quad (7)$$

that affords coefficients \mathbf{K}_I and energies ϵ_I for the I th eigenstate of the exciton Hamiltonian. Very recently, we derived and implemented analytic nuclear gradients and nonadiabatic couplings for this model,³² such that derivatives $H_{JK}^{[x]} \equiv \partial H_{JK} / \partial x$ can be readily computed and used to investigate which vibrational modes strongly modulate the coupling between eigenstates J and K .

Eigenvectors for a dimer of tetracene extracted from a DFT-optimized crystal structure (see the Supporting Information for details) are presented in Table 1. In the following, we have

Table 1. Eigenvectors for the Tetracene Dimer in the Nonorthogonal Exciton-Site Basis^a

eigenstate	$ \Xi_{S_0}\rangle$	$ \Xi_{S_1}\rangle$	$ \Xi_{S_2}\rangle$	$ \Xi_{TT}\rangle$
exc. energy (eV)		2.30	2.36	2.50
osc. strength		0.114	0.208	0.000
basis state	coefficient			
$ \Psi_A \Psi_B\rangle$	0.998	0.048	0.035	0.002
$ \Psi_A^* \Psi_B\rangle$	0.038	−0.994	0.227	−0.009
$ \Psi_A \Psi_B^*\rangle$	0.047	−0.225	−0.994	−0.011
$ ^1(TT)\rangle$	−0.001	−0.012	−0.010	1.114

^aA 50% truncation threshold for the NTOs.

corrected the site energies of the basis states to match the experimental values of 2.3 eV for the $S_0 \rightarrow S_1$ excitation energy and 2.5 eV for twice the S_0/T_1 gap. We find that the singly excited bright states $|\Xi_{S_1}\rangle$ and $|\Xi_{S_2}\rangle$ are primarily composed of a single basis state and that the optically dark multiexciton state, $|\Xi_{TT}\rangle$, is dominated by the triplet-pair basis state with only minor contributions from the singlet states. This is in agreement with other work²² and demonstrates that both the single- and multiexciton states can be characterized by a dominant electron configuration. Relatively weak electronic coupling between the singlet and triplet-pair basis states also

suggests that purely electronically coherent oscillations are unlikely to play a significant role in the SF mechanism.

Although the states in question are predominantly single-configuration (up to spin adaptation), mixing with CT configurations is thought to be important as electronic couplings between CT configurations and both single- and multiexciton configurations are about an order of magnitude larger than the direct coupling between $|S_0S_1\rangle$ and $|^1(TT)\rangle$.^{22,33} CT basis states $|\Phi_A^+\Phi_B^-\Phi_C\dots\rangle$ and $|\Phi_A^-\Phi_B^+\Phi_C\dots\rangle$ can easily be added to the exciton-site basis, with the resulting eigenvectors listed in Table 2. Our model predicts non-negligible couplings

Table 2. Eigenvectors for the Tetracene Dimer in the Nonorthogonal Exciton-Site Basis, Including CT Basis States^a

eigenstate	$ \Xi_{S_0}\rangle$	$ \Xi_{S_1}\rangle$	$ \Xi_{S_2}\rangle$	$ \Xi_{TT}\rangle$	$ \Xi_{-+}\rangle$	$ \Xi_{-+}\rangle$
exc. energy (eV)		2.30	2.39	2.50	2.69	3.16
osc. strength		0.185	0.114	0.011	0.025	0.010
basis state	coefficient					
$ \Psi_A\Psi_B\rangle$	0.996	0.000	0.045	0.041	-0.051	-0.049
$ \Psi_A^*\Psi_B\rangle$	-0.035	-0.875	0.224	0.308	-0.354	0.070
$ \Psi_A\Psi_B^*\rangle$	-0.045	0.164	0.972	0.000	0.177	-0.193
$ \Psi_A^+\Psi_B^-\rangle$	0.040	-0.448	-0.063	-0.346	0.821	-0.004
$ \Psi_A^-\Psi_B^+\rangle$	-0.025	-0.062	-0.163	0.145	0.011	-0.974
$ ^1(TT)\rangle$	0.002	-0.134	0.080	-0.970	-0.496	-0.170

^aA 50% truncation threshold for the NTOs.

between the excitonic and CT configurations, with both the single- and multiexciton eigenvectors gaining appreciable CT character. The presence of the CT configurations also leads indirectly to increased mixing of the single- and multiexciton states, acting as virtual intermediates, as predicted in several previous studies.^{8,18,21–23} The CT-dominated eigenstates, however, lie too high in energy to be accessed directly. Despite the slight increase in mixing, the character of the eigenstates remains predominantly single-configuration, suggesting that the presence of CT states is not sufficient to induce meaningful electronic coherence.

Nonadiabatic coupling vectors between $|\Xi_{S_1}\rangle$ and $|\Xi_{TT}\rangle$ are provided in the Supporting Information, using both 25 and 50% thresholds for truncating the natural transition orbitals (NTOs). This change in threshold results in a significant change in the norm of $\mathbf{H}_{JK}^{[x]}$, which more than doubles (from 5 to 10 au) when the tighter threshold is used. Tighter thresholds tend to stabilize exciton-site energies and increase coupling magnitudes, but the differences affect our results only qualitatively (see Tables S2 and S3 in the Supporting Information), at least in this system. As the resulting eigenstates are only slightly more mixed, this significant change in the norm of the derivative couplings reflects the sizable magnitudes of the quantities $\mathbf{H}_{JK}^{[x]}$. Inspection of the individual matrix elements, which contribute directly to the Hellman–Feynman part of \mathbf{h}^{JK} , can be quite significant in magnitude, ~ 100 au.

For intramolecular SF in 2-methyl-1,5-hexadiene, non-adiabatic couplings computed at the CASSCF(4,4) level are found to be as large as $\|\mathbf{h}\| = 172$ au at a particular intersection of the single- and multiexciton potential surfaces yet only 0.182 au at the ground-state geometry.³³ The situation is different in tetracene, however, given that the two potential surfaces do not

appear to cross in this system.^{22,34} It is therefore notable that we find $\|\mathbf{h}\| \approx 10$ au even at the ground-state geometry. This fact, along with the sizable geometry dependence of the elements of $\mathbf{H}_{JK}^{[x]}$, suggests significant nuclear/electronic coupling.

Projection of $\mathbf{H}_{JK}^{[x]}$ onto phonon modes can shed light on the nature of the vibrations that promote SF. Four high-frequency modes depicted in Figure 1a–d together constitute about 80% of the total projection, which seems sufficiently high to conclude that these are the primary modes that are driving the SF transition. There is a certain symmetry among these modes, consisting of two pairs of intramolecular vibrations localized on each of the two monomers. In pentacene, a conical intersection

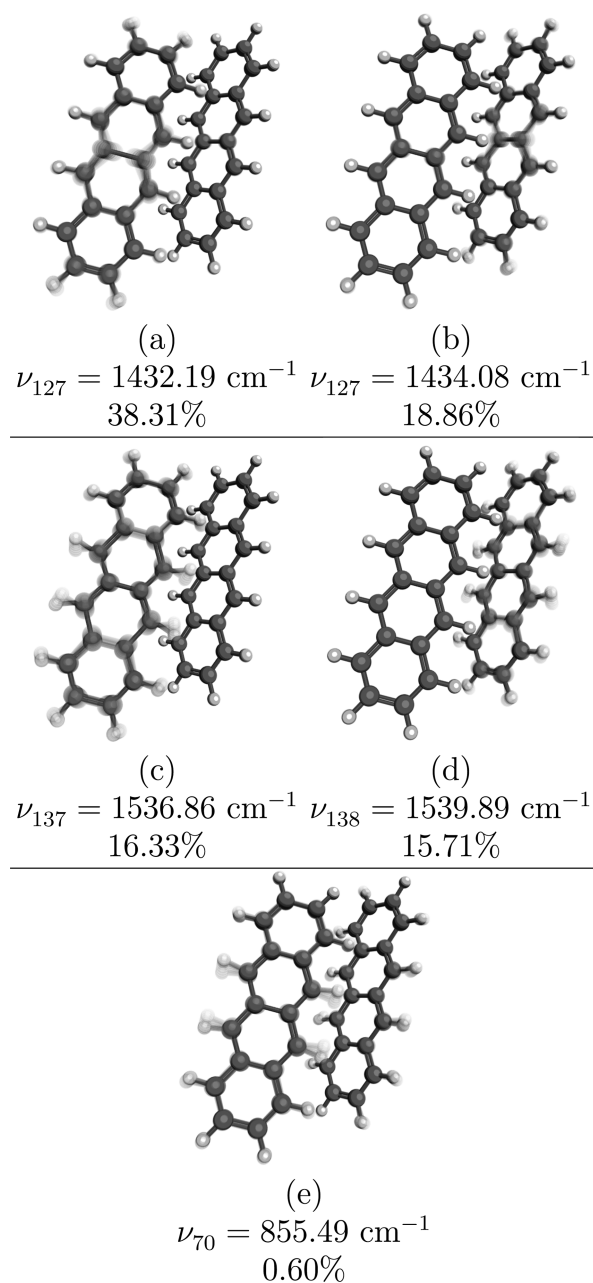


Figure 1. (a–d) Normal modes that strongly couple the S_1 and $^1(TT)$ states in the tetracene dimer, which together account for 80% of the norm of $\mathbf{H}_{JK}^{[x]}$. (e) Lowest-frequency vibration having any significant projection onto the nonadiabatic coupling vector.

along a low-frequency, intermolecular herringbone vibration has been identified,^{7,22} which would also modulate the electronic coupling, but we find no such intermolecular contribution in tetracene. The lowest-frequency vibration with any significant projection onto the nonadiabatic coupling vector is $\nu_{70} = 855 \text{ cm}^{-1}$ (Figure 1e), but although delocalized across the dimer, this mode is primarily a degeneracy-induced linear combination of intramolecular vibrations.

Electron/phonon coupling constants discussed in the context of charge transport in organic photovoltaics are, at their heart, derivatives of the matrix elements of an exciton Hamiltonian.³⁵ In this context, derivatives $H_{AA}^{[x]}$ are known as “Holstein” couplings and quantify the modulation of site energies due to nuclear motion, while off-diagonal derivatives $H_{A,B\neq A}^{[x]}$ (“Peierls” couplings) quantify how the electronic couplings (sometimes called “transfer integrals”¹⁶) change due to nuclear motion.^{35–38} Both types of couplings can be computed from the AIFDEM, by transforming $H_{AB}^{[x]}$ from nuclear Cartesian displacements to dimensionless spectroscopic coordinates for the respective normal modes.³² Results for the five normal modes in Figure 1 are presented in Table 3.

Table 3. Electron/Phonon Coupling Constants (in meV) for the Tetracene Dimer

basis state	$ \Psi_A \Psi_B\rangle$	$ \Psi_A^* \Psi_B\rangle$	$ \Psi_A \Psi_B^*\rangle$	$ ^1(\text{TT})\rangle$
$\nu_{70} = 855.49 \text{ cm}^{-1}$				
$ \Psi_A \Psi_B\rangle$	-30.726	-0.384	0.431	0.021
$ \Psi_A^* \Psi_B\rangle$	-0.384	-34.603	-0.038	-0.041
$ \Psi_A \Psi_B^*\rangle$	0.431	-0.038	-42.187	-0.010
$ ^1(\text{TT})\rangle$	0.021	-0.041	-0.010	10.570
$\nu_{127} = 1432.19 \text{ cm}^{-1}$				
$ \Psi_A \Psi_B\rangle$	-117.40	-3.9663	0.813	0.042
$ \Psi_A^* \Psi_B\rangle$	-3.966	65.772	-0.704	-0.084
$ \Psi_A \Psi_B^*\rangle$	0.813	-0.7043	-76.367	0.014
$ ^1(\text{TT})\rangle$	0.042	-0.084	0.014	182.907
$\nu_{128} = 1434.08 \text{ cm}^{-1}$				
$ \Psi_A \Psi_B\rangle$	76.788	-1.143	-4.858	-0.006
$ \Psi_A^* \Psi_B\rangle$	-1.144	101.989	0.824	0.035
$ \Psi_A \Psi_B^*\rangle$	-4.858	0.824	-96.317	0.017
$ ^1(\text{TT})\rangle$	-0.006	0.035	0.017	-98.108
$\nu_{137} = 1536.86 \text{ cm}^{-1}$				
$ \Psi_A \Psi_B\rangle$	7.124	4.509	-1.008	-0.042
$ \Psi_A^* \Psi_B\rangle$	4.509	-47.105	-0.620	0.094
$ \Psi_A \Psi_B^*\rangle$	-1.008	-0.620	-4.092	0.063
$ ^1(\text{TT})\rangle$	-0.042	0.094	0.063	-170.112
$\nu_{138} = 1539.90 \text{ cm}^{-1}$				
$ \Psi_A \Psi_B\rangle$	-16.454	-0.295	3.052	0.062
$ \Psi_A^* \Psi_B\rangle$	-0.295	-17.219	-0.723	-0.006
$ \Psi_A \Psi_B^*\rangle$	3.052	-0.7223	54.502	-0.029
$ ^1(\text{TT})\rangle$	0.062	-0.006	-0.029	139.292

It is immediately apparent that the dominant electron/phonon couplings for SF in tetracene are of the Holstein type, with the Peierls couplings being 10^3 – 10^4 times smaller. (Note that Holstein couplings are often called “local” couplings, but for the $|\Xi_{\text{TT}}\rangle$ state the wave function, and therefore the site energy, is a function of both monomers of the dimer.) Values of the Holstein coupling constants (~ 50 – 180 meV) are only

somewhat smaller than the $\sim 200 \text{ meV}$ energy gap between the single- and multiexciton eigenstates, and this is true even for ν_{70} , the lowest-frequency mode considered here.

In the context of charge transport, it is recognized that the nonlocal (Peierls) electronic couplings are coupled strongly to low-frequency intermolecular vibrations and can exhibit fluctuations of the same order of magnitude as the couplings themselves.³⁹ In contrast, for SF in tetracene, these couplings are insignificant and therefore too are their fluctuations. Instead, trends in electron/phonon couplings predicted by our model suggest that any vibronic character in the eigenstates involved in the SF transition is due to fluctuations in the site energies, with negligible modulation of the couplings.

The most striking result of the vibrational analysis is not apparent in the displacements shown in Figure 1 but rather in the frequencies of the modes in question, corresponding to excitation energies of 170–190 meV for the vibrational fundamentals. This makes vibrational excitation nearly resonant with the energy gap between the single- and multiexciton eigenstates. Indeed, of all of the vibrational modes, the five discussed here are the best match to the energy gap. Other studies have noted the importance of resonant bath modes in quantum dynamics simulations of SF in pentacene,^{8,40} although the vibrational frequencies in those simulations were resonant with the singlet to CT transition rather than the singlet to multiexciton transition. Recent experiments on pentacene support the participation of high-frequency vibrations to SF.^{6,41} Whereas Musser et al.⁶ propose a conical intersection along these driving modes—a pathway that existing calculations disfavor for tetracene—Bakulin et al.⁴¹ propose that these modes couple the single- and multiexciton states to form a set of vibronic states of mixed electronic character. The suggested mechanism is then a quantum-coherent one, as suggested also by Chan et al.,¹⁸ but one induced through vibronic resonance rather than purely electronic coupling.

To examine the possibility of a vibronic mechanism for SF, we use a model Hamiltonian of the Holstein–Peierls form,^{16,17} parametrized using our *ab initio* electronic and electron/phonon couplings, and phonon frequencies. Exciton-site energies are once again shifted so that excitation energies match experiment. We include a single vibrational degree of freedom (ν_{127}) as this mode has the largest projection along the nonadiabatic coupling vector. The basis used to diagonalize this model Hamiltonian consists of direct products of the AIFDEM electronic states with harmonic oscillators $|\chi_0\rangle$ and $|\chi_1\rangle$ having either 0 or 1 quanta in ν_{127} . The lowest vibronic eigenstates $|\Omega_n\rangle$ are listed in Table 4.

According to these calculations, the multiexciton-dominated dark state, $|\Omega_6\rangle$, falls higher in energy than that in the purely electronic case due primarily to excited vibrational character. Its energy is approximately $2[E(T_1) - E(S_0)] + h\nu_{127}$. The two lowest excited states, on the other hand, each possess appreciable oscillator strength and are essentially degenerate with the experimental S_1 state, yet are of decidedly mixed single- and multiexciton character, as well as mixed $|\chi_0\rangle$ versus $|\chi_1\rangle$ character, suggesting vibronic coherence.

We next use Redfield dissipative dynamics^{42–45} to investigate vibronic effects at a qualitative level. The Redfield approach has been used previously to study SF,^{8,18,41} and we have performed such simulations using three different Hamiltonians: purely excitonic, exciton + CT, and vibronic. In order to make a direct comparison between these models, we set the exciton-site

Table 4. Vibronic Eigenstates of a Holstein–Peierls Hamiltonian Parameterized Using AIFDEM Calculations^a

eigenstate	$ \Omega_0\rangle$	$ \Omega_1\rangle$	$ \Omega_2\rangle$	$ \Omega_3\rangle$	$ \Omega_4\rangle$	$ \Omega_5\rangle$	$ \Omega_6\rangle$
excitation energy (eV)		2.301	2.306	2.350	2.500	2.560	2.620
oscillator strength		0.0876	0.0727	0.0645	0.0184	0.0009	0.0013
basis state	coefficient						
$ \Psi_A \Psi_B\rangle X_0\rangle$	-0.998	0.038	-0.025	-0.035	-0.004	0.012	-0.001
$ \Psi_A^* \Psi_B\rangle X_0\rangle$	-0.037	-0.810	0.531	-0.194	0.250	-0.038	0.005
$ \Psi_A^* \Psi_B\rangle X_1\rangle$	0.001	0.199	-0.128	0.096	0.955	-0.251	0.012
$ \Psi_A \Psi_B^*\rangle X_0\rangle$	-0.046	-0.186	0.098	0.955	-0.114	-0.265	-0.000
$ \Psi_A \Psi_B^*\rangle X_1\rangle$	-0.001	-0.029	0.018	0.284	0.230	0.952	0.016
$ ^1(TT)\rangle X_0\rangle$	0.001	-0.538	-0.826	-0.016	0.012	0.010	-0.519
$ ^1(TT)\rangle X_1\rangle$	-0.000	0.281	0.436	0.014	0.013	0.009	-0.986

^aA 50% truncation threshold for the NTOs.

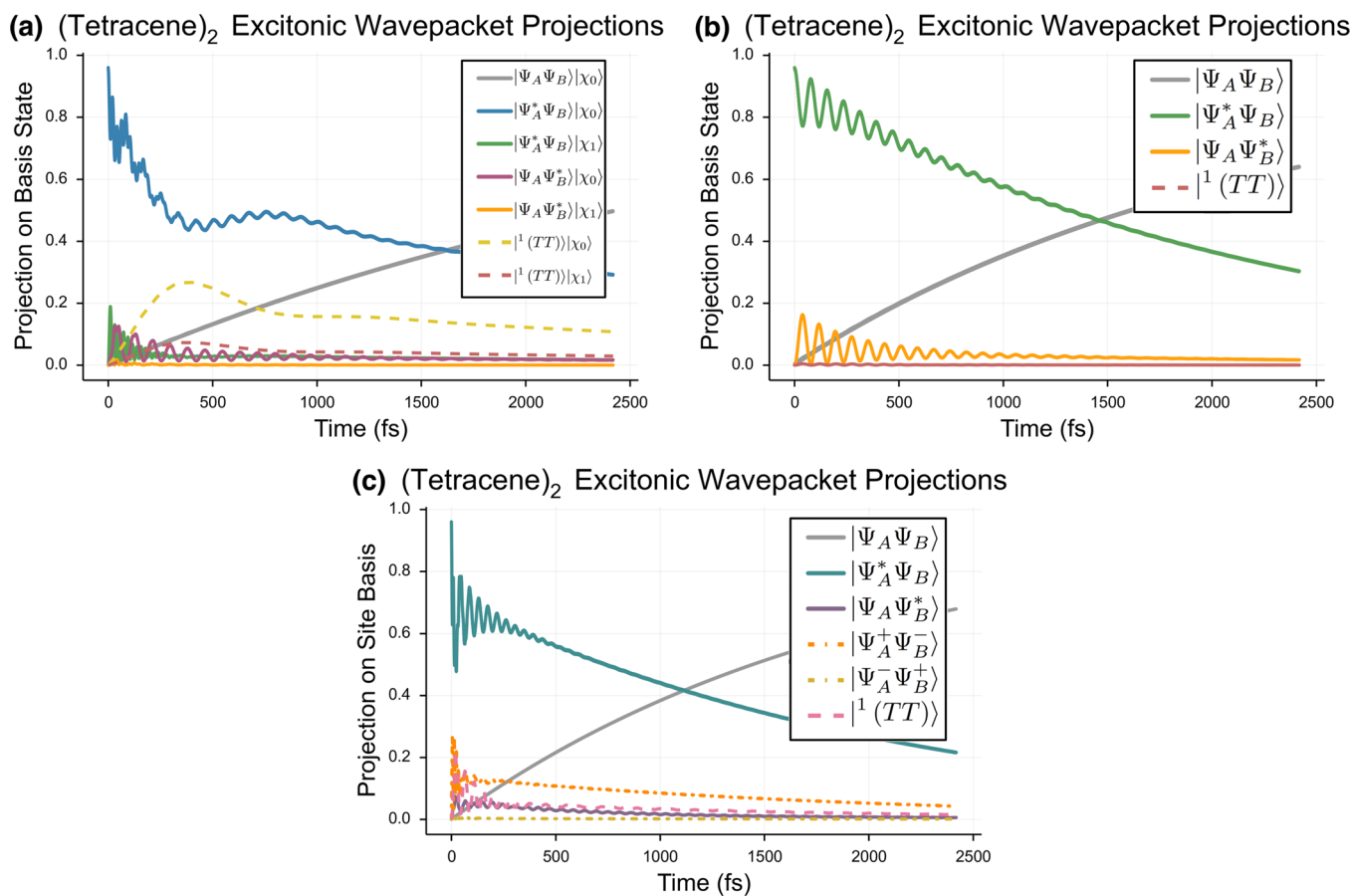


Figure 2. Redfield density matrix simulations using different model Hamiltonians: (a) vibronic, (b) purely excitonic, and (c) an excitonic model including CT states.

energies in all three cases equal to those computed in the vibronic case (Table 4). The goal is not to reproduce experimental results in the two purely electronic cases but to treat the three cases on an equal footing and thereby identify the role of vibronic coupling. All simulations use a common Ohmic spectral density to describe the vibrational modes (save for the one that is treated explicitly in the vibronic model) by means of a temperature bath with a reorganization energy of 0.3 eV and characteristic frequency of 1450 cm^{-1} . We initially populate the $|\Psi_A^* \Psi_B\rangle|X_0\rangle$ configuration and then propagate the

wave packet and plot its projection onto each basis state, in Figure 2.

It is immediately clear that the vibronic model is the only case where the wave packet spontaneously acquires multiexciton character, despite the electronic energy barrier. The exciton + CT model exhibits a small amount of initial multiexciton population, but this decays to zero almost immediately. Unsurprisingly, the purely excitonic model does not populate the multiexciton state at all. The vibronic model, in contrast, populates the multiexciton state on a time scale of ~ 0.5 ps, which is consistent with an ultrafast transition to an intermediate state with significant multiexciton character, as

suggested by Tayebjee et al.²⁰ and also observed experimentally;^{14,18} independent triplets are then accessed through a variety of pathways.^{9–11} We note that this is a simple model that does not describe all possible SF pathways, but these results suggest that vibronic coupling can provide sufficient impetus to overcome the unfavorable electronic energetics and motivate spontaneous, ultrafast SF in tetracene.

In summary, we have computed nonadiabatic couplings for crystalline tetracene, for the first time at an *ab initio* level of theory, finding that the coupling pertinent to the $|S_0S_1\rangle \rightarrow |^1(TT)\rangle$ SF transition is significant even at the ground-state geometry. Upon projecting the coupling vector onto phonon modes, we identify several *intramolecular* vibrational coordinates that strongly couple the single- and multiexciton states and whose vibrational fundamentals lie in near-resonance with the single- to multiexciton energy gap. *Ab initio* electron/phonon coupling constants computed for these modes are primarily of the Holstein type, serving to modulate the site energies rather than the intersite couplings. Dissipative dynamics simulations using a vibronic Hamiltonian parametrized from these *ab initio* calculations demonstrate that vibronic coupling among these intramolecular modes is sufficient to drive a spontaneous, ultrafast transition to the multiexciton state from which SF can proceed, despite an electronic energy gap. Although CT states do contribute as virtual intermediates, spontaneous SF is insignificant in the absence of vibronic coupling.

■ ASSOCIATED CONTENT

Supporting Information

The Supporting Information is available free of charge on the ACS Publications website at DOI: 10.1021/acs.jpcllett.7b00230.

Additional details about the calculations and derivative coupling data (PDF)

■ AUTHOR INFORMATION

Corresponding Author

*E-mail: herbert@chemistry.ohio-state.edu.

ORCID

John M. Herbert: 0000-0002-1663-2278

Notes

The authors declare the following competing financial interest(s): J.M.H. serves on the board of directors of Q-Chem, Inc.

■ ACKNOWLEDGMENTS

This work was supported by the U.S. Department of Energy, Office of Basic Energy Sciences, Division of Chemical Sciences, Geosciences, and Biosciences under Award No. DE-SC0008550. A.F.M. acknowledges a fellowship from the Lubrizol Corporation, and J.M.H. is a fellow of the Alexander von Humboldt Foundation. Calculations were performed at the Ohio Supercomputer Center under Project No. PAA-0003.⁴⁶

■ REFERENCES

- (1) Smith, M. B.; Michl, J. Singlet Fission. *Chem. Rev.* **2010**, *110*, 6891–6936.
- (2) Smith, M. B.; Michl, J. Recent Advances in Singlet Fission. *Annu. Rev. Phys. Chem.* **2013**, *64*, 361–386.
- (3) Tayebjee, M. J. Y.; McCamey, D. R.; Schmidt, T. W. Beyond Shockley Queisser: Molecular Approaches to High-Efficiency Photovoltaics. *J. Phys. Chem. Lett.* **2015**, *6*, 2367–2378.
- (4) Congreve, D. N.; Lee, J.; Thompson, N. J.; Hontz, E.; Yost, S. R.; Reuswig, P. D.; Bahlke, M. E.; Reineke, S.; van Voorhis, T.; Baldo, M. A. External Quantum Efficiency Above 100% in a Singlet-Exciton-Fission-Based Organic Photovoltaic Cell. *Science* **2013**, *340*, 334–337.
- (5) Jundt, C.; Klein, G.; Sipp, B.; Le Moigne, J.; Joucla, M.; Villaes, A. Exciton Dynamics in Pentacene Thin Films Studied by Pump-Probe Spectroscopy. *Chem. Phys. Lett.* **1995**, *241*, 84–88.
- (6) Musser, A. J.; Liebel, M.; Schnedermann, C.; Wende, T.; Kehoe, T. B.; Rao, A.; Kukura, P. Evidence for Conical Intersection Dynamics Mediating Ultrafast Singlet Exciton Fission. *Nat. Phys.* **2015**, *11*, 352–357.
- (7) Zimmerman, P. M.; Bell, F.; Casanova, D.; Head-Gordon, M. Mechanism for Singlet Fission in Pentacene and Tetracene: From Single Exciton to Two Triplets. *J. Am. Chem. Soc.* **2011**, *133*, 19944–19952.
- (8) Berkelbach, T. C.; Hybertsen, M. S.; Reichman, D. R. Microscopic Theory of Singlet Exciton Fission. II. Application to Pentacene Dimers and the Role of Superexchange. *J. Chem. Phys.* **2013**, *138*, 114103.
- (9) Burdett, J. J.; Müller, A. M.; Gosztola, D.; Bardeen, C. J. Excited State Dynamics in Solid and Monomeric Tetracene: The Roles of Superradiance and Exciton Fission. *J. Chem. Phys.* **2010**, *133*, 144506/1–144506/12.
- (10) Wilson, M. W. B.; Rao, A.; Johnson, K.; Gélinas, S.; di Pietro, R.; Clark, J.; Friend, R. H. Temperature-Independent Singlet Exciton Fission in Tetracene. *J. Am. Chem. Soc.* **2013**, *135*, 16680–16688.
- (11) Birech, Z.; Schwoerer, M.; Schmeiler, T.; Pflaum, J.; Schwoerer, H. Ultrafast Dynamics of Excitons in Tetracene Single Crystals. *J. Chem. Phys.* **2014**, *140*, 114501/1–114501/9.
- (12) Vaubel, G.; Baessler, H. Excitation Spectrum of Crystalline Tetracene Fluorescence: A Probe for Optically-Induced Singlet-Exciton Fission. *Mol. Cryst. Liq. Cryst.* **1971**, *15*, 15–25.
- (13) Thorsmølle, V. K.; Averitt, R. D.; Demsar, J.; Smith, D. L.; Tretiak, S.; Martin, R. L.; Chi, X.; Crone, B. K.; Ramirez, A. P.; Taylor, A. J. Morphology Effectively Controls Singlet-Triplet Exciton Relaxation and Charge Transport in Organic Semiconductors. *Phys. Rev. Lett.* **2009**, *102*, 017401/1–017401/4.
- (14) Chan, W.-L.; Ligges, M.; Zhu, X.-Y. The Energy Barrier in Singlet Fission can be Overcome Through Coherent Coupling and Entropic Gain. *Nat. Chem.* **2012**, *4*, 840–845.
- (15) Piland, G. B.; Bardeen, C. J. How Morphology Affects Singlet Fission in Crystalline Tetracene. *J. Phys. Chem. Lett.* **2015**, *6*, 1841–1846.
- (16) Coropceanu, V.; Cornil, J.; da Silva Filho, D. A.; Olivier, Y.; Silbey, R.; Brédas, J.-L. Charge Transport in Organic Semiconductors. *Chem. Rev.* **2007**, *107*, 926–952.
- (17) Zhugayevych, A.; Tretiak, S. Theoretical Description of Structural and Electronic Properties of Organic Photovoltaic Materials. *Annu. Rev. Phys. Chem.* **2015**, *66*, 305–330.
- (18) Chan, W.-L.; Berkelbach, T. C.; Provorov, M. R.; Monahan, N. R.; Tritsch, J. R.; Hybertsen, M. S.; Reichman, D. R.; Gao, J.; Zhu, X.-Y. The Quantum Coherent Mechanism for Singlet Fission: Experiment and Theory. *Acc. Chem. Res.* **2013**, *46*, 1321–1329.
- (19) Pensack, R. D.; Ostroumov, E. E.; Tilley, A. J.; Mazza, S.; Grieco, C.; Thorley, K. J.; Asbury, J. B.; Seferos, D. S.; Anthony, J. E.; Scholes, G. D. Observation of Two Triplet-Pair Intermediates in Singlet Exciton Fission. *J. Phys. Chem. Lett.* **2016**, *7*, 2370–2375.
- (20) Tayebjee, M. J. Y.; Clady, R. G. C. R.; Schmidt, T. W. The Exciton Dynamics in Tetracene Thin Films. *Phys. Chem. Chem. Phys.* **2013**, *15*, 14797–14805.
- (21) Mirjani, F.; Renaud, N.; Gorczak, N.; Grozema, F. C. Theoretical Investigation of Singlet Fission in Molecular Dimers: The Role of Charge Transfer States and Quantum Interference. *J. Phys. Chem. C* **2014**, *118*, 14192–14199.
- (22) Feng, X.; Luzanov, A. V.; Krylov, A. I. Fission of Entangled Spins: An Electronic Structure Perspective. *J. Phys. Chem. Lett.* **2013**, *4*, 3845–3852.
- (23) Casanova, D. Electronic Structure Study of Singlet Fission in Tetracene Derivatives. *J. Chem. Theory Comput.* **2014**, *10*, 324–334.

- (24) Berkelbach, T. C.; Hybertsen, M. S.; Reichman, D. R. Microscopic theory of singlet fission. III. Crystalline pentacene. *J. Chem. Phys.* **2014**, *141*, 074705/1–074705/12.
- (25) Elliott, P.; Goldson, S.; Canahui, C.; Maitra, N. T. Perspective on Double-Excitations in TDDFT. *Chem. Phys.* **2011**, *391*, 110–119.
- (26) Matsika, S.; Feng, X.; Luzanov, A. V.; Krylov, A. I. What We Can Learn from the Norms of One-Particle Density Matrices, and What We Can't: Some Results for Interstate Properties in Model Singlet Fission Systems. *J. Phys. Chem. A* **2014**, *118*, 11943–11955.
- (27) Feng, X.; Krylov, A. I. On Couplings and Excimers: Lessons from Studies of Singlet Fission in Covalently Linked Tetracene Dimers. *Phys. Chem. Chem. Phys.* **2016**, *18*, 7751–7761.
- (28) Morrison, A. F.; You, Z.-Q.; Herbert, J. M. Ab Initio Implementation of the Frenkel-Davydov Exciton Model: A Naturally Parallelizable Approach to Computing Collective Excitations in Crystals and Aggregates. *J. Chem. Theory Comput.* **2014**, *10*, 5366–5376.
- (29) Morrison, A. F.; Herbert, J. M. Low-Scaling Quantum Chemistry Approach to Excited-State Properties Via an *Ab Initio* Exciton Model: Application to Excitation Energy Transfer in a Self-Assembled Nanotube. *J. Phys. Chem. Lett.* **2015**, *6*, 4390–4396.
- (30) Herbert, J. M.; Zhang, X.; Morrison, A. F.; Liu, J. Beyond Time-Dependent Density Functional Theory Using Only Single Excitations: Methods for Computational Studies of Excited States in Complex Systems. *Acc. Chem. Res.* **2016**, *49*, 931–941.
- (31) Mayhall, N. J. From Model Hamiltonians to Ab Initio Hamiltonians and Back Again: Using Single Excitation Quantum Chemistry Methods to Find Multiexciton States in Singlet Fission Materials. *J. Chem. Theory Comput.* **2016**, *12*, 4263–4273.
- (32) Morrison, A. F.; Herbert, J. M. Analytic Derivative Couplings and Electron/Phonon Couplings for an *Ab Initio* Frenkel-Davydov Exciton Model: Application to Triplet Exciton Mobility in Crystalline Tetracene. In preparation.
- (33) Havenith, R. W. A.; de Gier, H. D.; Broer, R. Explorative Computational Study of the Singlet Fission Process. *Mol. Phys.* **2012**, *110*, 2445–2454.
- (34) Zimmerman, P. M.; Musgrave, C. B.; Head-Gordon, M. A Correlated Electron View of Singlet Fission. *Acc. Chem. Res.* **2013**, *46*, 1339–1347.
- (35) Girlando, A.; Grisanti, L.; Masino, M.; Bilotti, I.; Brillante, A.; Della Valle, R. G.; Venuti, E. Peierls and Holstein Carrier-Phonon Coupling in Crystalline Rubrene. *Phys. Rev. B: Condens. Matter Mater. Phys.* **2010**, *82*, 035208/1–035208/8.
- (36) Troisi, A. Prediction of the Absolute Charge Mobility of Molecular Semiconductors: The Case of Rubrene. *Adv. Mater.* **2007**, *19*, 2000–2004.
- (37) Hannewald, K.; Stojanović, V. M.; Schellekens, J. M. T.; Bobbert, P. A.; Kresse, G.; Hafner, J. Theory of Polaron Bandwidth Narrowing in Organic Molecular Crystals. *Phys. Rev. B: Condens. Matter Mater. Phys.* **2004**, *69*, 075211/1–075211/7.
- (38) Hannewald, K.; Bobbert, P. A. *Ab Initio* Theory of Charge-Carrier Conduction in Ultrapure Organic Crystals. *Appl. Phys. Lett.* **2004**, *85*, 1535–1537.
- (39) Troisi, A.; Orlandi, G. Dynamics of the Intermolecular Transfer Integral in Crystalline Organic Semiconductors. *J. Phys. Chem. A* **2006**, *110*, 4065–4070.
- (40) Tamura, H.; Huix-Rotllant, M.; Burghardt, I.; Olivier, Y.; Beljonne, D. First-Principles Quantum Dynamics of Singlet Fission: Coherent Versus Thermally Activated Mechanisms Governed by Molecular π Stacking. *Phys. Rev. Lett.* **2015**, *115*, 107401/1–107401/5.
- (41) Bakulin, A. A.; Morgan, S. E.; Kehoe, T. B.; Wilson, M. W. B.; Chin, A. W.; Zigmantas, D.; Egorova, D.; Rao, A. Real-Time Observation of Multiexcitonic States in Ultrafast Singlet Fission Using Coherent 2D Electronic Spectroscopy. *Nat. Chem.* **2015**, *8*, 16–23.
- (42) Redfield, A. G. In *Advances in Magnetic and Optical Resonance*; Waugh, J. S., Ed.; Academic Press, 1965; Vol. 1; pp 1–32.
- (43) Breuer, H.-P.; Petruccione, F. *The Theory of Open Quantum Systems*; Oxford University Press, 2002.
- (44) Schröter, M. *Dynamics in Light Harvesting Complexes*, 1st ed.; BestMasters; Springer Spektrum, 2015.
- (45) Valkunas, L.; Abramavicius, D.; Mančal, T. *Molecular Excitation Dynamics and Relaxation*; Wiley-VCH Verlag GmbH and Co. KGaA: Weinheim, Germany, 2013.
- (46) Ohio Supercomputer Center. <http://osc.edu/ark:/19495/f5s1ph73> (accessed March 7, 2017).